nature methods

Review article

https://doi.org/10.1038/s41592-024-02564-4

Probing the physical hallmarks of cancer

Received: 8 February 2024

Accepted: 11 November 2024

Published online: 15 January 2025

Check for updates

Hadi T. Nia [1] ✉, Lance L. Munn [2] ✉ & Rakesh K. Jain [2] ✉

The physical microenvironment plays a crucial role in tumor development, progression, metastasis and treatment. Recently, we proposed four physical hallmarks of cancer, with distinct origins and consequences, to characterize abnormalities in the physical tumor microenvironment: (1) elevated compressive–tensile solid stresses, (2) elevated interstitial fluid pressure and the resulting interstitial fluid flow, (3) altered material properties (for example, increased tissue stiffness) and (4) altered physical micro-architecture. As this emerging field of physical oncology is being advanced by tumor biologists, cell and developmental biologists, engineers, physicists and oncologists, there is a critical need for model systems and measurement tools to mechanistically probe these physical hallmarks. Here, after briefly defining these physical hallmarks, we discuss the tools and model systems available for probing each hallmark in vitro, ex vivo, in vivo and in clinical settings. We finally review the unmet needs for mechanistic probing of the physical hallmarks of tumors and discuss the challenges and unanswered questions associated with each hallmark.

The tumor microenvironment surrounding cancer cells plays a critical role in tumor initiation, progression, metastasis and treatment response. During growth, tumors not only disturb the structure and function of the adjacent tissue but also co-opt normal cells from the nearby environment. This recruitment of normal cells leads to further changes in matrix and cellular composition within the tumor. This results in physical abnormalities in both cancer cells and the tumor microenvironment that not only fuel tumor progression and metastasis but also confer resistance to various treatments (Table 1). The direct and indirect links between tumor biology and physics have provided new opportunities for the discovery of new mechanisms underlying tumor progression, immune evasion and treatment resistance.

To provide a conceptual framework for cancer, we recently proposed four physical hallmarks of cancer[1]: (1) elevated solid stress, (2) elevated interstitial fluid pressure (IFP), (3) increased stiffness and altered material properties and (4) abnormal micro-architecture. These four physical hallmarks are conceptually distinct, having different causes and consequences, and they enable and synergize with many of the biological hallmarks to facilitate cancer cell expansion, invasion and evasion of immune attack. Solid stresses are created as a growing tumor pushes and stretches solid components of the surrounding tissue (Fig. 1 and Table 1). Solid stresses are distinct from fluid pressure, and they are almost zero in most normal tissues. However, solid stresses are large enough to compress blood and lymphatic vessels in and around tumors, causing hypoxia and low pH[2–7]. Elevated IFP is caused by leakage of plasma from abnormally permeable tumor blood vessels and insufficient lymphatic drainage (Fig. 2 and Table 1). The resulting abnormal fluid dynamics make it difficult to deliver drugs to the tumor and can enhance angiogenesis and metastasis[8]. Increased stiffness is caused by matrix deposition and remodeling (Fig. 3 and Table 1). Tissue stiffness, either equilibrium stiffness or time-dependent stiffness (viscoelasticity), has been linked to several hallmarks of cancer[9,10]. Finally, when normal tissue architecture is disrupted by cancer, there is altered micro-architecture as normal and cancer cells lose association with their lumens and basement membranes and as matrix components adopt new configurations (Fig. 4 and Table 1). How these changes in the interactions between an individual cell and its surrounding matrix and neighboring cells facilitate invasion and metastasis is not fully understood, in part due to a lack of widely accepted and validated methods to measure them. We aim to fill this gap by critically evaluating current and emerging tools and model systems to probe the physical hallmarks of cancer.

We begin each section with the definition and description of each physical hallmark followed by a summary of its biological importance

[1]Department of Biomedical Engineering, Boston University, Boston, MA, USA. [2]Steele Laboratories, Department of Radiation Oncology, Massachusetts General Hospital and Harvard Medical School, Boston, MA, USA. ✉e-mail: htnia@bu.edu; lmunn@mgh.harvard.edu; rjain@mgh.harvard.edu

Table 1 | Methods of measuring and altering the physical hallmarks of cancer

	Method	Setting	Scale/resolution	Advantages	Limitations	Ref.
Methods to probe solid stress	Partial cut	Ex vivo measurement	Whole mouse/human tumor	Versatile, can be performed with minimal training	Provides a rough estimate of solid stress. Appropriate to show the existence of solid stress	5
	Planar cut	Ex vivo measurement	Whole mouse/human tumor at the resolution of imaging modalities, for example, 30 μm via high-res ultrasound	Provides a 2D map of solid stresses in resected mouse and human tumors	Requires imaging modalities such as 3D ultrasound or optical imaging	2,6,128
	Slicing	Ex vivo measurement	Whole mouse/human tumor at the resolution of imaging modalities, for example, 30 μm via high-res ultrasound, 1 μm with optical microscopy	A sensitive method to measure small levels of solid stress in resected tumors and normal organs with residual stresses. This method is more sensitive than planar cut.	Requires imaging modalities such as 3D ultrasound or optical imaging	2,128,129
	Biopsy punch	Ex vivo, in situ measurement	Whole mouse/human tumor at the resolution of imaging modalities, for example, 30 μm via high-res ultrasound	Provides a 1D profile of solid stresses without the need to resect the tumor from the host organ. This method captures the stresses applied by the host organ to the tumor.	Requires imaging modalities such as 3D ultrasound or optical imaging	2,128
	Elastic microgel	In vivo, in situ, ex vivo, in vitro measurement	Resolution of imaging modality, for example, submicrometer using a multiphoton microscope. Temporal resolution can be real time over multiple days. In mice, temporal resolution is determined by the anesthesia limit: a couple of hours per day.	In vivo measurement of solid stresses; longitudinal tracking of solid stresses by tumor growth and response to treatment	Measures solid stresses at the location of the beads; not applicable to early stages of tumor formation; limitation in imaging depth	7,33–35
	Oil microdroplet	In vivo, in vitro measurement	Resolution of imaging modality, for example, submicrometer using a multiphoton microscope. Temporal resolution can be real time over multiple days.	Allows measurement of anisotropic stresses that make the oil droplet change shape	Does not measure isotropic components of stress; the injection process may induce artifacts.	128
	Embedding spheroids in hydrogel	In vitro application	At the scale of cellular and multicellular aggregates. Temporal resolution can be real time over multiple days.	Simple; spheroid generates forces intrinsically.	Solid stress depends on spheroid growth/metabolism.	11,36
	Applying osmotic stress	In vitro application	At the scale of cellular and multicellular aggregates	Adjustable level of stress; versatile technique for any size of spheroids	May cause cell swelling due to osmosis	39
	Applying stress on the cell monolayer	In vitro application	Monolayer of adherent cells. Confluency is not needed.	Controlled level of solid stress without increasing hypoxia as a common confounding factor	Stress application is 2D, not 3D.	14
	Plating cells in a pre-stressed substrate	In vitro application	Monolayer of adherent and confluent cells	Controlled level of in-plane solid stress	The stresses are in plane and 2D; the cells may detach if the stress is high.	40,130
	Applying chronic stress with mechanical system	In vivo application	Stress application area of a few millimeters; the deformation resolution on the order of submillimeters.	In vivo and chronic application of stress on normal tissues simulating the stresses applied by the growing tumors	The stress is applied in 2D on the organ of interest, not in 3D, which normal tissue experiences from growing tumors.	6,15
	Applying chronic stress with magnetic nanoparticles	In vivo application	Stress application area depends on the magnet area, commonly a few millimeters.	In vivo and chronic stress by embedding magnetic particles inside cells	It depends on the cellular uptake of nanoparticles by the cell.	16

https://doi.org/10.1038/s41592-024-02564-4

Table 1 (continued) | Methods of measuring and altering the physical hallmarks of cancer

	Method	Setting	Scale/resolution	Advantages	Limitations	Ref.
Methods to probe fluid pressure	'Wick-in-needle'	In vivo (preclinical and clinical)	Measurement at only the point of needle insertion; resolution of sub-mmHg with common sensors up to maximum systolic blood pressure	Versatile method to measure fluid pressure in clinical and preclinical models; measures fluid pressure independent of solid stresses	One time point; challenging for longitudinal measurement of pressure	43
	Micropipette method	In vivo	Measurement at only the point of needle insertion; resolution of sub-mmHg with common sensors up to maximum systolic blood pressure	Accurate measures of fluid pressure with minimal tissue damage	One time point; challenging for long-term longitudinal measurements	43
	Micropore chamber	In vivo	Measurement of flow at the bulk tumor	Measures alteration in fluid pressure longitudinally over several days in the preclinical setting (for example, mouse models of cancer)	Animal only; not appropriate for tumors that are smaller than the chamber	58
	Mathematical modeling	In vivo, in silico	Resolution depends on the experimental methods to acquire the pressure.	Inferring fluid flow from the known pressure	Requires the material's properties such as hydraulic permeability	57
	FRAP	In vivo (preclinical), in vitro	Measurement at optical resolution, that is, cellular level	High-resolution flow measurement using fluorescent microscopy	Limited to the surface of tumors due to limited depth of optical imaging	59
	MRI-based imaging	In vivo (preclinical and clinical)	Whole-organ scale but with resolution of submillimeters	Measures fluid flow in 3D noninvasively. The whole organ can be imaged in clinical and preclinical settings.	Low resolution of flow field. Only measures flow, not pressure. Estimating pressure requires mathematical modeling.	60
	Flow chambers and transwell inserts	In vitro	Cellular events at high cellular numbers could be phenotyped.	Application of fluid shear stresses. Appropriate when a large number of cells are needed for molecular biology assays	Application of fluid shear stress on cell monolayer, not 3D tumors. Lacks real-time imaging capabilities	53
	Microfluidic devices	In vitro	Appropriate for a limited number of cells that can be imaged in a given region of interest via optical imaging	Application of highly controlled fluid flow and pressure; 2D and 3D models. Two or more cell types can be co-cultured with tunable matrix properties.	Limited number of cell types due to intrinsic co-culture limitations. Shallow depth of optical imaging	49–51

https://doi.org/10.1038/s41592-024-02564-4

Table 1 (continued) | Methods of measuring and altering the physical hallmarks of cancer

	Method	Setting	Scale/resolution	Advantages	Limitations	Ref.
Methods to probe stiffness	AFM/optical/magnetic tweezers	In vitro, ex vivo	Cellular and subcellular resolution. Scale is limited to a single cell or a few cells wide.	High-resolution measurement of stiffness	Limited to surface measurement (2D) or locally measured for isolated individual cells	2,64,75
	Dynamic indentation	In vitro, ex vivo	Depending on the measurement method, can be cellular (AFM) or tissue scale (macro-indenter)	Measuring viscoelasticity	The time scale of indenter (limited often by resonance frequency of the actuator) needs to be smaller than viscoelastic time constants that need to be measured.	62
	Macroscale compression and shear tests	Ex vivo, in vitro	Tissue scale that reports a bulk value per specimen	Gold standard of stiffness measurement	Requires bulk tissue, often resected	57
	Laser speckle rheology	In situ, ex vivo	Cellular and multicellular resolution	Contactless, high-resolution measurement of stiffness, minimal invasiveness	Requires mathematical models to estimate stiffness	81
	Brillouin scattering	In vivo, in vitro	Cellular and subcellular resolution	Contactless, high-resolution measurement of stiffness, minimal invasiveness	Reports hydromechanical properties on the order of GPa; much higher values than kPa-level stiffness values	82
	μElastography	Ex vivo, in vitro	Cellular- to whole-organ-scale measurement at optical resolution	3D high-resolution measurement of stiffness using thermo-responsive hydrogels	Requires embedding of samples inside thermo-responsive hydrogels; longitudinal measurements not possible	83
	Ferrofluid microdroplet embedding	In vivo	Cellular measurement at the point of microdroplet insertion	In vivo deformation and inference of mechanical properties by applying a magnetic field	Local measurement only at the point where the microdroplet is embedded; requires injection of the microdroplet with potential injection artifacts	131
	MR/ultrasound elastography	In vivo, ex vivo	Whole-organ scale at submillimeter resolution. High-resolution ultrasound has limited depth of a few millimeters but with resolution of 30–70 μm.	3D full-organ map of stiffness	Estimates shear wave speed or speed of the sound; requires inferring of stiffness with knowledge of tissue density or other properties	84,85
	Optical elastography via crystal ribcage	Ex vivo	Optical resolution, whole tumor and whole organ (lung)	3D map of tumor stiffness in a functioning lung	Limited depth of imaging due to optical imaging	7,41,79
	2D hydrogels with tunable stiffness values	In vitro	Single-cell imaging analysis to multicell molecular biology assays	Highly controlled stiffness values with a large dynamic range	Only applicable for 2D cell monolayers	63
	3D hydrogels with tunable stiffness values	In vitro	Single-cell imaging analysis to multicell molecular biology assays	Controlled stiffness values in 3D	May affect pore size	10,64, 88–92
	3D hydrogel overlaid on 2D substrates with tunable stiffness	In vitro	Single-cell imaging analysis to multicell molecular biology assays	Controlled 3D hydrogel with desired composition while stiffness is controlled via the substrate	While cells are cultured in 3D, stiffness sensing is in 2D.	95
	3D culture systems with controlled cross-linkers	In vitro	Single-cell imaging analysis to multicell molecular biology assays	Controlled stiffness values without affecting pore size	Limited dynamic range of stiffness values	67,94
	Alginate hydrogel modified with PEG	In vitro	Single-cell imaging analysis to multicell molecular biology assays	Controlling viscoelasticity while keeping the equilibrium elasticity constant	Challenges in dissecting intrinsic viscoelasticity (scale independent) versus poroelasticity (scale dependent)	10

https://doi.org/10.1038/s41592-024-02564-4

Table 1 (continued) | Methods of measuring and altering the physical hallmarks of cancer

	Method	Setting	Scale/resolution	Advantages	Limitations	Ref.
Methods to probe architecture and cell geometry	Histological analysis and SHG	Ex vivo, in vitro, in situ	Subcellular resolution for the whole tumor section	Labeled or label-free imaging of tissue architecture at optical resolution	Limited depth of view due to optical imaging	3,41,100, 116,117
	SHG through crystal ribcage	Ex vivo in functioning lung	Subcellular imaging of the whole tumor in a functioning lung	Altered architecture in a functioning lung; allows longitudinal studies	Limited depth of view due to optical imaging	41
	3D pathology (CODA)	Ex vivo (fixed/ embedded samples)	Subcellular resolution in fixed or frozen tissue	3D high-resolution architecture of tissues applicable to paraffin-embedded samples	Altered architecture due to serial sectioning and the embedding process	118
	Altered adhesion of the substrate	In vitro	Cellular resolution (optical imaging)	Controlled cell geometry by controlling substrate adhesion	Applicable mainly to 2D cell culture	104,105
	Micropillar and nanopillar substrates	In vitro	Cellular resolution (optical imaging)	Altering cell adhesion while having independent control of substrate stiffness	2D systems	106
	Altering nucleus geometry	In vitro	Cellular resolution (optical imaging)	Altered substrate adhesion properties and area	2D systems	109
	Migration through pores in microfluid systems	In vitro	Cellular resolution (optical imaging) with a limited number of cells	Altered nucleus geometry recapitulating cell migration through constrictions; allows optical imaging of the dynamic events	2D systems	107,110,111
	Transwell inserts	In vitro	Imaging application is challenging but appropriate for molecular biology assays due to high cell number.	Altered nucleus geometry recapitulating cell migration through constrictions; allows for high-throughput assays	2D systems	110
	Nano/micro-grooved surfaces	In vitro	Cellular resolution (optical imaging) with a limited number of cells	Highly controlled nano/ micro-architecture	2D systems	107,114
	Altering network alignment in 3D hydrogels	In vitro	Cellular resolution with optical imaging capabilities. Application to both single-cell and spheroid embedding	Probing the response to altered architecture in 3D	Altered architecture may also change stiffness properties as a confounding factor.	123,124

High-res, high resolution; 1D, one dimensional.

https://doi.org/10.1038/s41592-024-02564-4

https://doi.org/10.1038/s41592-024-02564-4

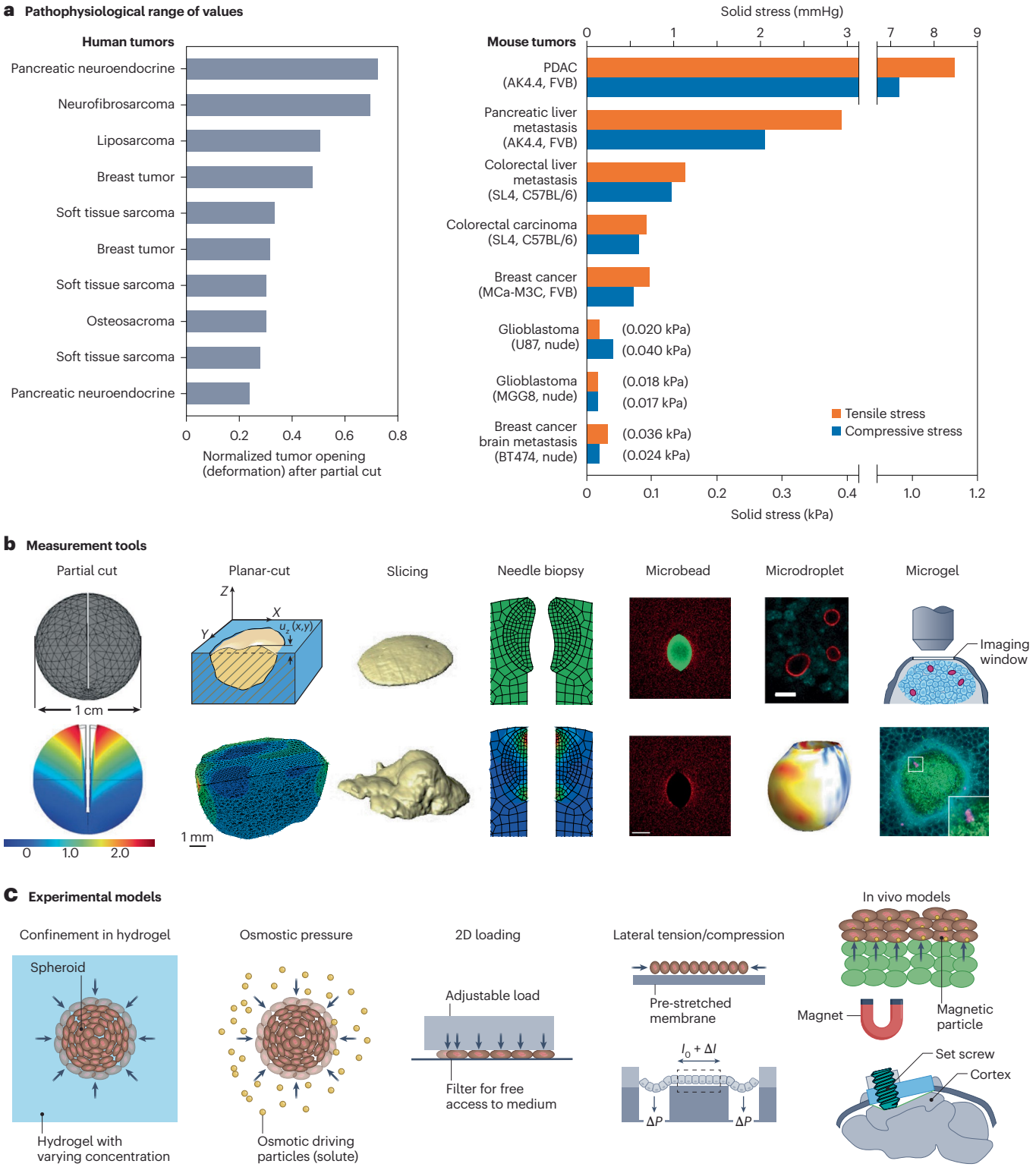

Fig. 1 | Solid stress, range of values, measurement tools and experimental model systems. a, The pathophysiological range of values of compressive and tensile stress in human[5] and mouse tumors[3,6]. The repeated tumor types are from different patients. **b**, Measurement tools for quantifying solid stress include partial cut[5], planar cut[3], slicing[3], needle biopsy[3], microbeads[36] and microgels[7,33–35], demonstrated through intravital imaging[7] and crystal ribcage[41]. **c**, Experimental model systems include growth of spheroids in hydrogels[11], osmotic pressure applied to spheroids[39], compression of cell monolayers[14], pre-stretch of cell monolayers[40], stretching cells by swelling of a membrane[130], confined growth of cells in 3D hydrogels[132], application of chronic compression to colon tissue in vivo using magnetic nanoparticles[16] and mechanical devices for applying chronic compression to brain tissue[6] or lymph nodes[15]. *l*, length; *P*, pressure. Photographs reproduced with permission from the following: **b**, partial cut, ref. 5, PNAS; planar cut, slicing and needle biopsy, ref. 3, Springer Nature Limited; microbead, ref. 12 under a Creative Commons license CC BY 4.0; microdroplet, ref. 46, Springer Nature America; microgel, ref. 7, Springer Nature Limited; **c**, in vivo models, ref. 24, Springer Nature Limited.

https://doi.org/10.1038/s41592-024-02564-4

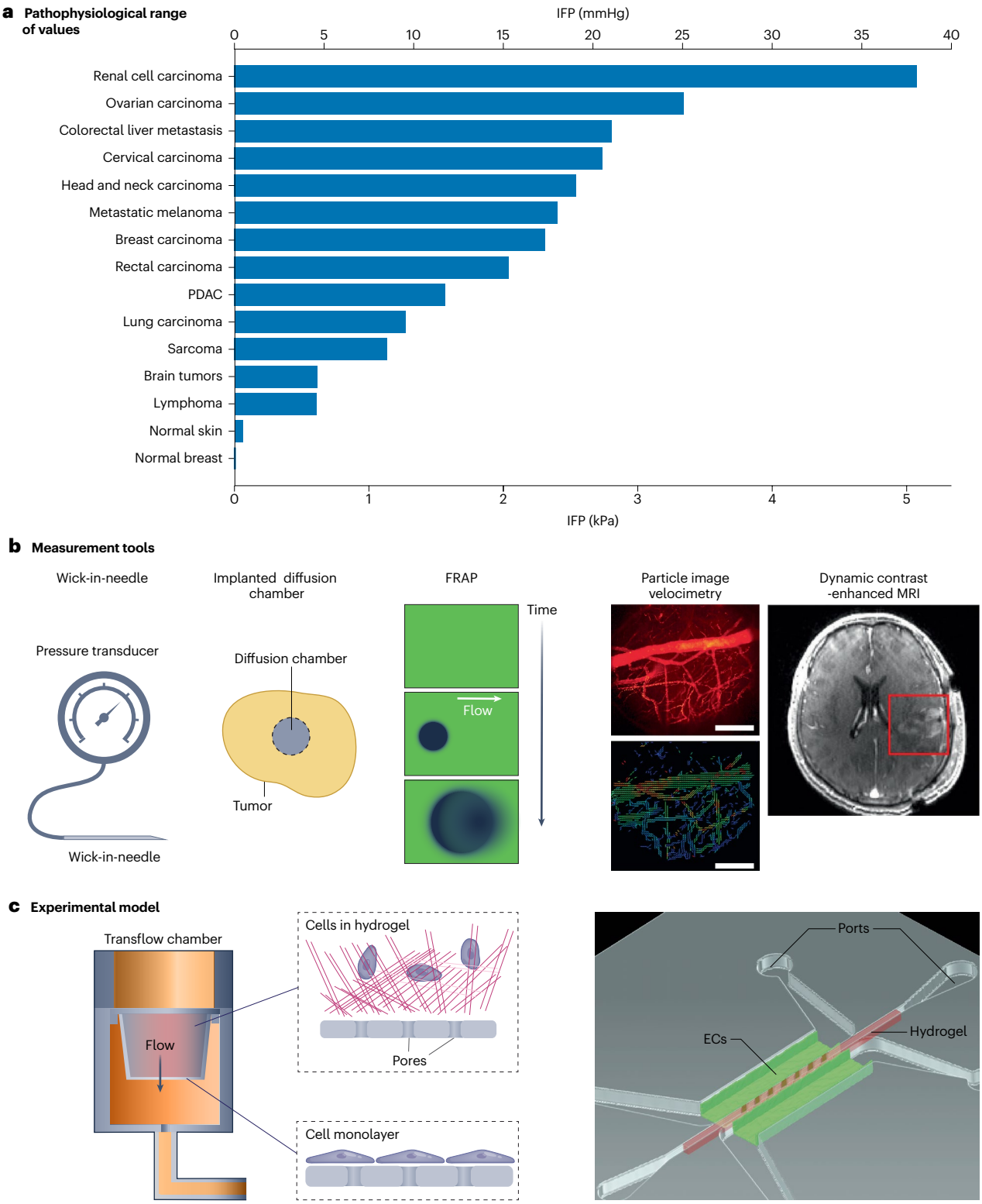

Fig. 2 | IFP and interstitial fluid flow, range of values, measurement tools and experimental model systems. a, Pathophysiological range of IFP values in human tumors[43]. **b**, Measurement tools used to quantify IFP and interstitial fluid flow include wick-in-needle or micropipette[43], implanted diffusion chamber in rodents[58], FRAP[59], particle image velocimetry[61] and dynamic contrast-enhanced MRI[60]. **c**, Experimental model systems to study IFP and interstitial flow in vitro include transflow chambers and microfluidics[49,50]. ECs, endothelial cells. Photographs in **b** reproduced from the following: particle image velocimetry, ref. 50, Springer Nature Limited; axial, ref. 51, Springer Nature.

https://doi.org/10.1038/s41592-024-02564-4

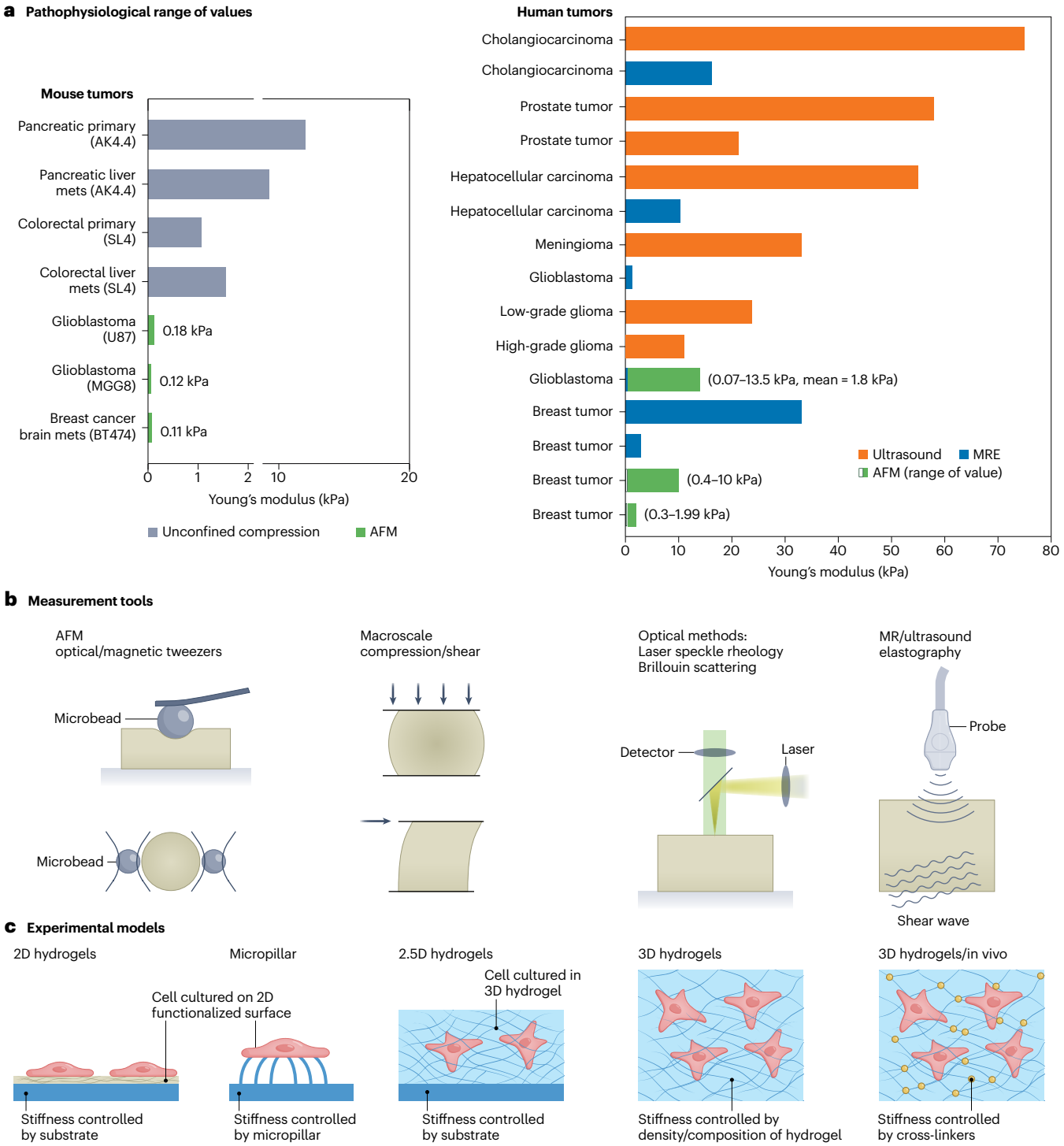

Fig. 3 | Stiffness (rigidity), range of values, measurement tools and experimental model systems. a, The pathophysiological range of values in mouse and patient tumors: cholangiocarcinoma (ultrasound[84]), hepatocellular carcinoma (ultrasound[84], MR[85]), prostate cancer[133], breast cancer (AFM[71], MRE[134]), meningioma, low-grade glioma, high-grade glioma, normal brain[135], glioblastoma (AFM)[70], glioblastoma (MRE[136]). Range of stiffness values in mouse tumors: primary and metastatic pancreatic and colorectal tumors[3]; glioblastoma and breast cancer brain metastasis (mets)[6]. **b**, Measurement tools for quantifying stiffness include AFM and optical or magnetic tweezers[3,62,137], macroscale compression and shear tests[57], optical methods such as laser speckle rheology[81], Brillouin scattering[82] and μElastography[83] and MR or ultrasound elastography[84,85,136]. **c**, Experimental model systems for studying stiffness include monolayer 2D culture on substrates with controlled stiffness[63], 3D culture in a hydrogel overlaid on substrates with controlled stiffness, 3D culture systems with controlled material density and stiffness properties[64] and 3D culture systems with controlled cross-linking[67].

and clinical relevance. We then describe the existing tools to quantify these hallmarks in patients, animal models and in vitro model systems, which have played an important role in identifying the origin and revealing the importance of physical abnormalities in the microenvironment. The final section describes the experimental model systems available for mechanistic studies of each hallmark.

https://doi.org/10.1038/s41592-024-02564-4

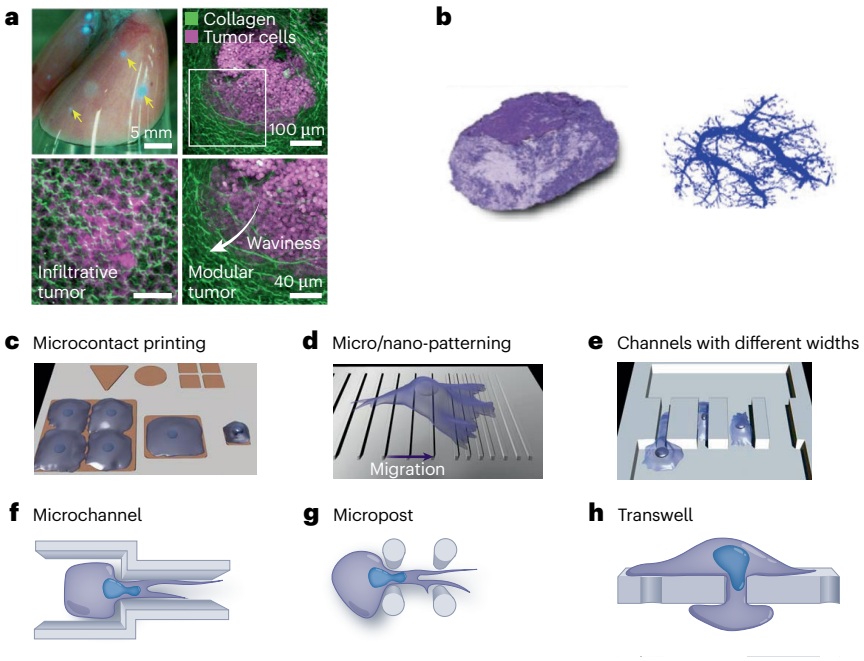

Fig. 4 | Architecture and geometry: representative observations and experimental model systems. a,**b**, Representative observations. **c**–**h**, Experimental model systems. **a**, Linking structure to function in infiltrative versus nodular tumors via SHG in a lung metastasis imaged through crystal ribcage[41]. Nodular tumors stretch collagen around the tumor, while infiltrative tumors preserve the wavy collagen architecture. **b**, An example of 3D pathology reconstructed H&E images from the CODA platform, which enables visualization of tumor architecture in 3D[118]. **c**, Studying cellular response, for example, proliferation, apoptosis and migration, in response to changes in the geometry of the cells and their surroundings is made possible via microcontact printing for a wide range of cellular responses[138]. **d**, Nanofabrication is used to engineer substrate architecture and its effect on cell migration, a mode of migration termed topotaxis[114]. **e**, Channels with different widths and aspect ratios are used to probe cell response to geometry and confinement; channel compliance can also be modified[122]. **f**–**h**, Microchannels, microposts and transwells are used as model systems to control architecture and consequently cell and nucleus geometry during migration[106,107,114]. Photographs reproduced from the following: **a**, ref. 17, Springer Nature America; **b**, ref. 116, Springer Nature America.

Solid stresses and elastic energy

Biological tissues are composed of two phases: a solid phase that includes the extracellular matrix (ECM) and solid constituents such as cell membranes and cytoskeletons and a fluid phase, which includes blood and lymph as well as interstitial and intracellular fluids. When pushed or pulled, solid elements resist the force, and, if they have elasticity, they can store some of the energy (think of a spring being stretched or compressed). Similarly, solid elements can resist shear forces. Solid stresses are the mechanical forces (compressive, tensile and shear) contained in and transmitted by solid and elastic elements of the ECM and cells rather than fluids[11]. Solid stresses are also known as residual stresses, as they remain unrelaxed in tissues and can store mechanical energy. Originating in physics, the term 'stress' is defined as a force normalized by area, with units of pascals (Pa) (1 mmHg = 133.322 Pa). In mouse tumor models, solid stress values range from less than 100 Pa in glioblastomas to 1,000 Pa in pancreatic ductal adenocarcinomas (PDACs; Fig. 1a). In human tumors, substantial levels of solid stress have been reported, assessed by measuring the deformation of ex vivo tissues after stress relaxation[5], but more precise measurements are needed by converting the deformation to stress values.

It is crucial to recognize that solid stress, a mechanical force, differs fundamentally from elasticity (stiffness) and viscoelasticity (time-dependent stiffness). Stiffness and viscoelasticity define how much or how fast a tissue will deform under an applied force, respectively. By contrast, solid stress is itself a latent force that results in stored energy. If a tissue contains solid stresses, it will undergo deformation when the stress is released (for example, through the methods discussed below). A biological sample can be stiff (rigid) or soft (compliant), and, regardless of its stiffness, it can be under compressive or tensile solid stresses[3] or be stress free as in most normal tissues. If the tissue is stress free, the relaxation of stress does not result in any deformation regardless of how stiff or soft the tissue is and regardless of how viscoelastic the tissue is. Solid stress can be compressive, as when it compresses blood vessels, and tensile, as seen when wavy collagen fibers become stretched. Solid stress, the forces transmitted or contained in the solid phase of the tissue, is also distinct from fluid pressure, the force applied through the fluid phase: there can be increased solid stress with no change in fluid pressure and vice versa.

Importance in cancer

The influence of solid stress on the biology of cancer cells was initially identified in 1997 by Helmlinger and colleagues, who discovered that the accumulation of solid stress limits the in vitro growth of tumor spheroids[11]. It was quickly realized that such stresses exist in vivo and that they are sufficiently large to compress and impair blood and lymphatic vessels[12]. Vessel compression contributes to hypoxia and low pH[4,5] and interferes with the delivery as well as the efficacy of chemotherapies, radiotherapies and immunotherapies[13]. Solid stress may also have more direct effects on tumor biology. For example, the application of compressive forces on a cell monolayer in vitro promotes invasiveness of cancer cells[14] and the application of mechanical stress in vivo can impair infiltration of lymphocytes[15] and stimulate tumorigenic pathways, for example, increasing β-catenin signaling in colon epithelia[16].

Because the matrix components retain solid stresses, numerous associated issues can be mitigated by using therapies that break down matrix and diminish fibrosis. For example, losartan, an angiotensin receptor 1 blocker, reduces fibrosis by (1) inhibiting transforming

growth factor (TGF)-β, required for collagen production by fibroblasts, and (2) blocking the function of connective tissue growth factor (CTGF), required to stabilize collagen fibers, and downregulating hyaluronan synthases 1–3 to lower hyaluronic acid (HA) levels[4]. In preclinical models of PDAC, losartan alleviates solid stress and decompresses blood vessels, improving blood flow, resulting in improved delivery and efficacy of chemotherapy, leading to increased overall survival[4]. It should be noted that reducing matrix production can also result in less stiffness, which is discussed in Stiffness (elasticity) and viscoelasticity. This strategy was tested in a phase 2 trial and led to unprecedented improvement in the resection rates of locally advanced PDAC treated with chemoradiotherapy[17]. However, this strategy failed when combined with immunotherapy in a randomized clinical trial (NCT01821729). Losartan also increased the efficacy of immunotherapy in murine models of glioblastoma, a uniformly fatal disease, when all randomized phase 3 trials of immunotherapy have failed[18]. Other tumors that have benefited from losartan include ovarian cancer and neurofibromatosis type 2 schwannomas[19,20].

Similarly, based on encouraging preclinical data[21], targeting the vitamin D receptor is currently being tested in patients (NCT03472833). Because PDAC tumors have high levels of HA, treatment with pegylated hyaluronidase (PEGPH20)[22] alleviated the compressive forces on blood vessels and increased overall survival when combined with chemotherapy[4]. Hyaluronidase also improves treatment efficacy in colorectal liver metastasis when combined with anti-VEGF agents and chemotherapy[23]. However, PEGPH20 has failed in all clinical trials to date[24]. Inhibiting the vitamin D receptor, which reduced markers of inflammation and fibrosis[21], and blocking Sonic Hedgehog signaling[25] improved blood flow and the outcome of chemotherapy in pancreatic tumors in mice, presumably as a result of decreased solid stress, but failed in a clinical trial. Collectively, these results suggest that we need a better understanding of the origins of solid stress and targetable elements to reduce solid stresses. Another gap of knowledge is the consequences of solid stress in tumors and the differential effect it may have on cancer versus normal cells to leverage strategies that decrease different components of the ECM of tumors to improve the treatment outcome in patients with desmoplastic tumors, which constitute ~20% of all human tumors.

Finally, solid stresses, whether as static intratumoral stresses or cyclic stresses generated by circulation and respiration cycles, play a substantial role in the activation of innate immune cells and their interactions with cancer cells through the activation of piezo ion channels[26]. More recently, the impact of stretch-activated piezo1 channels on adaptive immunity, for example, $CD4^+$ and regulatory T cells[27], has been reported in the context of cancer, wound healing and infectious diseases. Abnormal mechanics of tumors and their surrounding tissues, which may provide a new form of danger signal to both innate and adaptive immune cells, provide potential targets to regulate mechano-immunity of the tumor microenvironment[28–30].

Measurement techniques

Studying cardiovascular tissue in the 1980s, Fung noticed that the arterial wall relaxes and deforms when it is cut surgically because it contains 'residual' solid stresses[31]. He showed that the relaxation can be used to measure the intrinsic solid stress. The same approach can be used to estimate solid stress in tumors by partially cutting into a tumor and measuring the relaxation at the location of the cut[5] (Fig. 1b). This method can give an estimate of solid stress after making mathematical assumptions about tissue geometry, tissue mechanical properties and the distribution of solid stress.

More reliable measurements can be made if the cutting method is well defined and tissue stiffness is independently measured[3,32]. Recently, the experimental and mathematical frameworks of three such methods have been developed: the planar cut method, which allows two-dimensional (2D) mapping of solid stress in tumors; the slicing method, which provides a sensitive estimate of solid stress in small tumors with low levels of solid stress; and the needle biopsy method, which provides quantification of solid stress ex vivo and in situ (Fig. 1b). In the needle biopsy method, the tumor can be still embedded in the host organ; therefore, the mechanical confinement of the tumor and stromal tissue by host tissue remains intact[6]. Each of the three techniques uses the principle of controlled release of solid stress with precise geometry, followed by measurement of the resulting deformation through high-resolution ultrasonography or optical microscopy. Considering the distinctive patterns of stress relaxation, alongside the tumor's geometric and material characteristics, the distribution of compressive and tensile solid stress as well as the released elastic energy are calculated using mathematical models[3]. (Fig. 1b). These methods are capable of only measuring the tensile and compressive components of solid stress. Methods for quantifying the shear component of solid stress, a component with potential influence on biological responses of cells, remain to be developed. The above methods can be applied to tumors with arbitrary geometry and are accurate over a wide range of solid stress levels from a few pascals to tens of kilopascals. However, these methods are limited to only ex vivo or in situ measurements, for which the measurement is performed after the tissue is surgically removed. Hence, in comparison to in vivo measurement of solid stress[7] (see the paragraph below), ex vivo measurements may not represent the full range of solid stresses. Efforts to develop tools for measuring solid stress in vivo in human or preclinical tumor models are needed.

It is also possible to estimate solid stress by measuring the deformation of fluorescent oil microdroplets that have been injected into the tissue of interest. In tissues with negligible solid stress, the droplets remain spherical when there is negligible solid stress but change shape when solid stresses have deformed the tissue. This method has the advantage that it can be used in vivo and is sensitive at micrometer length scales. However, because it relies on optical microscopy to record drop morphology, there are depth penetration limitations. In addition, injecting the microdroplets may mechanically disrupt the tissue or biologically affect cells, and the method is insensitive to isotropic stresses, as oil droplets are incompressible. Another method, which incorporates elastic microgels made from hydrogels in vivo[7] and in vitro[7,33–35], addresses the incompressibility issue of the oil microdroplet method. When cell aggregates are formed around the compressible microgel, the solid stress generated during spheroid growth changes the diameter of the beads, which can be imaged via confocal microscopy and represents an indicator of solid stress. The solid stress exerted externally on a spheroid in a hydrogel can also be measured by tracking the microparticles embedded in the confining hydrogel[36]. While these works quantify solid stress generated collectively by multicellular aggregates, similar approaches have been used to measure the dynamic forces that a single cell generates during division[37] (Fig. 1b). For methods to measure solid stress or mechanical forces at the cellular and subcellular scales, using traction force microscopy, micropillars or molecular sensors (for example, fluorescence resonance energy transfer), we refer the reader to a relevant review paper[38].

Experimental model systems

The solid stress within the core of most tumors is compressive and relatively isotropic (the same in all directions), while the stress at the outer rim is mostly anisotropic, a combination of circumferential tension and radial compression. There are multiple experimental models for applying various mechanical stresses to tumors in vitro and in vivo. To simulate the isotropic forces inside a tumor, one simple approach is to grow cancer spheroids in hydrogels that have tunable elastic properties and with no adhesion ligands such as agarose[11] (Fig. 1c). As the spheroids grow due to proliferation and matrix deposition, the surrounding agarose gel is displaced. As the gel resists the displacement, the spheroid will experience solid stress that is proportional to the elastic constant ('stiffness') of the agarose and its displacement, caused by growth of the spheroid. Agarose displacement can be determined by quantifying the

volume change of the spheroid or alternatively by embedding fluorescent particles in the hydrogel that can be tracked microscopically[36] to determine the deformation field. However, it should be noted that, due to strain-stiffening phenomena, the stiffness of the spheroid may also change under solid stresses. Another way to apply isotropic solid stress is through the application of osmotic stresses externally to cell aggregates[39]. The osmotic pressure is applied by adding dextran (100 kDa) to the medium. The outer layer of the cellular aggregate restricts the penetration of particles into the spheroids, creating an osmotic force across the spheroid boundary. This method is capable of applying up to 20 kPa of stress isotropically (that is, uniformly from all directions) on spheroids. This method is more controllable in terms of adding dextran and controlling the solid stress level, while solid stress in the method of growing spheroids in agarose depends on the growth rate of spheroids.

To recapitulate the anisotropic stress field at the tumor margin[6,7], where cells are predominately compressed in the radial direction and are being effectively pressed against the surrounding tissue, it is possible to place defined weights on cells in culture. The cells are plated onto a filter to provide nutrients and oxygen from the bottom of the plate, independent of the loading, and a piston or platen with defined weight is placed on top. It is also possible to apply anisotropic force in the plane of the monolayer by plating the cells on a pre-stretched membrane where the compressive force is aligned with cell–cell interfaces. When the pre-stress is released, the membrane contracts, applying in-plane compressive forces on the cells[40]. However, it should be noted that the application of anisotropic solid stresses may represent stresses at the tumor periphery where there is tension–compression anisotropy at the interface of tumor–host tissue. To model solid stresses in the tumor core, systems that apply more isotropic stresses remain to be developed. The challenge with developing such models is to apply isotropic stresses without affecting the delivery of oxygen and nutrients so that the biological consequences of solid stresses are not confounded with pathways activated by hypoxia and starvation due to altered diffusion of oxygen and nutrients (Fig. 1c).

Finally, solid stress can be applied in vivo in mouse models by incorporating magnetic particles into the tissue (Fig. 1c). For example, colon tissue loaded with magnetic particles can be pulled by a magnet implanted subcutaneously in a mouse[16]. The cells that are pulled toward the magnet experience compressive solid stress and are biologically altered toward a tumorigenic phenotype[16]. In more recent work, an in vivo model system was developed to model the compressive forces that primary and metastatic tumors exert on their surrounding normal brain. The model consisted of a set screw mounted through a cranial window to apply controlled deformation of the underlying tissue, recapitulating the impact of tumor growth on normal brain tissue. This model system was used to test strategies to protect neurons against solid stress generated by brain tumors[6]. In brain tumors[6] and lung metastasis[41], it has been shown that growth patterns, that is, infiltrative, in which cancer cells diffuse into the normal tissue, versus nodular growth, in which the tumor grows as a cohesive nodule, give rise to different levels of solid stresses in the tumor and its surrounding tissue. Therefore, tumor growth patterns could be used for a deeper understanding of the causes and consequences of solid stresses.

IFP and interstitial fluid flow

Fluid pressure is another type of mechanical stress, with units of pascals (or mmHg due to the tradition of measuring fluid pressure using a column of mercury; 1 mmHg ≅ 133.3 Pa). In addition to the widely investigated flow of fluids within the blood and lymphatic networks, fluid also flows through the interstitium, that is, spaces within tissues not occupied by cells[1]. IFP is generally higher in tumors than in normal tissue and ranges from less than 1 kPa in brain tumors to 5 kPa in renal cell carcinomas (Fig. 2a). Leakage of fluid from abnormal tumor blood vessels and the inability of dysfunctional lymphatics to absorb this fluid increases IFP in the tumor, and the pressure difference between one region of tissue to another region causes interstitial flow, exposing the tissue to shear stresses that can influence its biology.

Importance in cancer

In 1988, we first predicted mathematically[42] and confirmed it experimentally in 1990 (ref. 43) that IFP is uniformly elevated throughout a tumor and drops precipitously in the margin with adjacent normal tissue, creating steep pressure gradients at the tumor periphery[42,43]. This causes fluid to percolate out of the tumor into the peritumor tissue, carrying with it growth factors and anti-tumor drugs, causing edema and aiding tumor progression[1]. IFP has been proposed as a prognostic marker in some clinical studies[44], and anti-VEGF agents, which reduce the leakiness of tumor vessels, reduce IFP in both rectal and breast tumors in patients[45,46]. Pressure-driven interstitial fluid flow generates shear stresses at cell surfaces, which can be estimated via mathematical modeling[47]. These shear stresses affect the biology of cancer cells as well as stromal cells in several ways, including activation of fibroblasts[48], modulating endothelial sprouting[49] and mediating invasion[50] and migration of cancer cells[51].

IFP and the shear stresses caused by interstitial fluid flow affect both cancer and stromal cells[52]. Shear stresses activate β-catenin signaling in cancer cells and stimulate oncogenic signaling pathways[53]. They also upregulate TGF-β expression and increase the activation and contraction of myofibroblasts[52], which results in matrix reorganization and stiffening. By inducing migration of stromal and cancer cells, shear stress can facilitate cancer invasion and angiogenesis[50,51]. Fluid flow can also skew cytokine concentrations and may encourage metastasis by transporting solutes and cancer cells toward low-pressure areas at the periphery of the tumor[54]. Given that immune cells react to interstitial flow, it is likely that the fluid shear forces play a role in the regulation of immune responses as well[52]. Interstitial fluid flow also affects angiogenesis[55] and lymphangiogenesis[52], as endothelial morphogenesis during sprouting has been shown to be directed by fluid flow. It is commonly assumed that shear stresses affect cell migration merely due to fluid flow, as the viscosity of interstitial fluid is often assumed constant throughout the tissue. However, more recently, it was shown that increased viscosity has a substantial effect on cancer cell migration through activation of transient receptor potential cation vanilloid 4 (TRPV4), which increases RhoA-dependent cell contractility[56].

In addition to the mechanotransduction activated by fluid shear stress, increased IFP also has an impact on tumor physiology through mechanisms including the transport of growth factors and cells. When IFP is high inside the tumor, the pressure difference between blood and the interstitial space is close to zero[55]. This hinders the convection of drugs from the vasculature into the tumor tissue[54]. Because there are functional lymphatic vessels in the normal tissue surrounding the tumor, the IFP there is near zero. This sets up a steep pressure gradient at the periphery of the tumor, which drives convective flux of interstitial fluid flow from the tumor toward the surrounding tissue. This outward interstitial flow promotes tumor invasion and growth by facilitating the transport of cancer cells and growth factors to the surrounding normal tissue[54]. The outward fluid flow also conveys therapeutic agents out of the tumor and hence reduces drug retention times[54].

Measurement techniques

The gold standard technique for measuring fluid pressure in vivo is the 'wick-in-needle' method. This technique uses a pressure transducer connected to a probe, which consists of a wick contained within a syringe needle or a glass micropipette (Fig. 2b). This probe can be inserted into the tissue to measure fluid pressure, independent of solid stresses[43]. By measuring IFP at multiple locations, it is possible to calculate the gradient of the fluid pressure ∇p and the fluid velocity $\mathbf{U}$ using Darcy's law, $\mathbf{U} = -k\nabla p$. This calculation requires information about the hydraulic permeability of the tissue, k. The hydraulic permeability of the tissue has an inverse relationship with desmoplasia; that

is, tumors with higher matrix density have greater resistance to fluid flow and hence a lower hydraulic permeability[57]. For large tumors, a diffusion chamber can be implanted inside the tumor where the high fluid pressure can be measured directly by tumor growth or in response to treatment[58].

Measurements of fluid flow can be made in vivo by tracking an appropriate tag or marker in the interstitium. Fluorescent recovery after photobleaching (FRAP) is a technique based on this concept, in which some of the fluorescent molecules in the interstitium are photobleached using a high-power, focally directed laser and the recovery of fluorescence into the bleached area is recorded. The bleached spot generally translates spatially as it disappears, allowing calculation of convection independent of diffusivity[59] (note that diffusion is a process governed by the random walk of particles in a solution, while, in convection, that is, pressure-induced flow, particles travel by the motion of the solution). Similar measurements can be made using magnetic resonance (MR) contrast agents[60]. For convective flows, for which there are distinct fiducial markers to track, such as red blood cells or added fluorescent particles, particle image velocimetry could be used to map the velocity field associated with pressure differences in the tumor and its surrounding environment[61]. Different modalities based on MR imaging (MRI) provide non-invasive and useful information about fluid flow and velocity in the interstitial space. Phase-contrast MRI is one approach that provides fluid velocity, and diffusion-weighted MRI is another method that provides diffusivity (mobility) of water in tumors[60] (Fig. 2b). Despite these advances, reliable IFP measurements remain invasive, and tumor IFP values for patients are only available for tumors that can be easily accessed by the wick-in-needle probe. There is a knowledge gap in interpreting clinical images, such as in fluid-attenuated inversion recovery images in which bright regions are often interpreted as edema. The development of non-invasive and validated techniques is needed to fill this gap.

Experimental model systems

Flow chambers and transwell inserts have been extensively used to apply controlled fluid pressure and fluid flow to cells plated in 2D or seeded in three-dimensional (3D) hydrogels[53] (Fig. 2c). With the advent of microfabrication technology, researchers now have more control over the flow configuration, and microfluidic devices are amenable to high-resolution imaging. Consequently, microfluidic devices are the most widely used tools for studying biological fluid flows in various settings[49–51].

Stiffness (elasticity) and viscoelasticity

Stiffness, also known as rigidity or elastic modulus, is an intrinsic material property. It is defined as the resistance of the material to deformation in response to an applied force. The proportional (normalized) deformation is known as strain, and the force per unit of area is known as stress. With these definitions, the elastic modulus of a material is the ratio of stress to strain; in other words, it is the amount of force required to deform the object by a certain amount. The unit of elastic modulus is the pascal. Elastic modulus values for human tumors are variable, ranging from less than 1 kPa in brain tumors to up to 70 kPa in cholangiocarcinomas (Fig. 3a).

Viscoelasticity (time-dependent elasticity) is also an intrinsic material property of the tissue or cells, which should not be confused with solid stress. Viscoelasticity defines the resistance of the material to deformation in response to an applied force at a predefined rate. Most soft tissues, including tumors, exhibit greater resistance to force (for example, greater stiffness) when the force is applied at high rates[10,62].

Consequences and importance in cancer

The best recognized and most tangible mechanical abnormality in tumors is increased tissue stiffness (Fig. 3). Unlike solid or fluid mechanical stresses, which describe a state of the tissue exposed to a force, stiffness is an intrinsic material property of the tissue. In a seminal study in 2006, sensing of stiffness by cells was implicated in determining cell lineage[63]. There are currently numerous studies showing how material properties, such as the stiffness of the microenvironment, are central to many hallmarks of cancer including proliferation[64], metabolism[65], angiogenesis[66], invasion[67] and migration, and metastasis[68].

The ECM often becomes stiffer during tumor development and progression, and this can facilitate malignancy. Stiffening promotes tumor progression in many tumor types including breast[64], pancreatic[69], colorectal[23] and brain tumors[70]. Additionally, increased stiffness promotes cancer cell invasiveness[67], induces invasion and metastasis[9], enhances immune cell infiltration[28,71], facilitates the epithelial–mesenchymal transition through TGF-β[72], alters growth factor secretion and signaling and increases angiogenesis and vessel permeability[66]. More recently, stiffening the ECM through glycation has been linked to increased tumor growth, providing a biomechanical link by which diabetic hyperglycemia promotes breast tumor progression[73].

Substantial evidence suggests that increased stiffness in breast tissue is associated with a greater risk of breast cancer[74], and mammographic density, which is strongly correlated with tissue stiffness, has been proposed as a predictor of poor survival[75]. In PDAC, increased stiffness negatively correlates with response to chemotherapy[69]. While stiffening has often been correlated with increased malignancy in cancer cells, in the case of bone metastases, higher bone density dampens metastatic progression through the attenuation of integrin-mediated mechanosensing[76].

Viscoelasticity is another stiffness-related material property, and its role has been studied in the context of mechanobiology in cancer and regenerative medicine[10]. Viscoelasticity, in general, constitutes intrinsic viscoelasticity, which is scale and fluid flow independent, and poroelasticity, which is both scale and fluid flow dependent. Chaudhuri et al. developed a hydrogel based on alginate, modified with polyethylene glycol (PEG) as a spacer to modulate the viscoelastic properties of the hydrogel while keeping the equilibrium elasticity constant[77]. In later works, reviewed comprehensively by Chaudhuri et al.[10], the contribution of viscoelasticity has been discussed in the context of cells sensing the mechanical properties of their microenvironment in 2D and 3D.

Physical hallmarks of cancer may interact and affect each other. For example, these mechanical stresses can alter the stiffness and architecture of the matrix through strain-stiffening[78,79] or because of nodular tumor growth that causes local expansion and stretching of the ECM[3,41]. These tensile stresses increase the stiffness of collagen fibers, which in turn further activates the focal adhesion contractility of cancer-associated fibroblasts in their vicinity, leading to a vicious cycle of matrix deposition and stiffening.

Currently, many researchers rely on pan-cancer analyses using matrisome libraries or genomic sequencing data to detect changes in the ECM as well as the cytoskeleton[80]. While useful for inferring mechanical changes in the tumor microenvironment, they do not provide direct measurements of the physical parameters.

Methods of measurement

Palpation has long been used to identify stiff tumors embedded in compliant tissue, especially in accessible locations such as the breast and skin. Palpation is based on the qualitative assessment of how much the tissue moves in response to a given force applied by the fingers or hand. It is possible to use this same concept to measure stiffness quantitatively ex vivo over a wide range of length scales (Fig. 3b). At the macroscale, the elasticity modulus can be measured via unconfined and confined compression and shear tests[57]. At the microscale and the nanoscale, atomic force microscopy (AFM)[3,62,70] and optical and magnetic tweezers use microscopic probes to manipulate cells, proteins or membranes to measure elasticity moduli[78]. Optical-based methods have been developed to analyze viscoelastic[81] and hydromechanical properties[82] of tissues and cells with high spatial resolution. More

recently, a thermo-responsive material has been used to deform tumor spheroids in 3D, and, using optical imaging coupled with mathematical modeling, the 3D stiffness map of the sample has been reported at optical resolution[83]. Many of these methods are difficult to perform in vivo and therefore rely on cell cultures or ex vivo sample preparation. However, several methods have been developed to quantify stiffness in tumors in vivo, such as ultrasound electrography[84] and MR electrography (MRE)[85]. Because stiffness is highly heterogeneous in tumors, as seen in Fig. 3a,b, an important unmet need is the measurement of stiffness of the whole tumor or the whole organ at high spatial resolution that can capture the heterogeneities. Methods such as AFM can map stiffness at subcellular resolution, however, through a limited region of interest that spans usually up to ten cells. Methods such as MRE map stiffness but usually at submillimeter resolution. More recently, methods such as μElastorgraphy using optical microscopy have been developed to bridge the gap between resolution and measurement extent with the potential to map the stiffness of whole-organ samples (for example, lymph node) at optical resolution[83]. Finally, measurements of tissue viscoelasticity with higher sensitivity and resolution have been made possible using high-frequency AFM[62]. While numerous methods are available to measure the stiffness of biological samples at different scales and resolutions, a remaining challenge is comparing these values across scales. The highly heterogeneous values reported and the differences between macroscale methods such as MRE and microscale methods such as AFM can also be attributed to methodology and sample preparation. Hence, it is essential to use consistent methods when changes in stiffness are to be evaluated in response to any interventions.

Experimental model systems

Unlike solid stress and IFP, where experimental methods are limited, several experimental model systems exist for simulating tissues with various elastic and viscoelastic properties to recapitulate this mechanical aspect of the tumor microenvironment. For example, plating cells on polyacrylamide gels with various Young's moduli results in differentiation along various lineages[63]. This highlights the central role that tissue stiffness plays in development. By controlling cross-linking, polyacrylamide gels can be prepared with a wide range of elastic moduli from 0.05 kPa to 100 kPa[63], mirroring the pathophysiological ranges of elastic constants in different tumors. Polyacrylamide gels are also easy to use for imaging and cell collection[64]. However, many signaling cues are lost in 2D cultures systems, and 3D culture systems are required to restore these signaling pathways[86]. Three-dimensional culture systems can implement multiple natural materials such as collagen[64], fibrin, reconstituted basement membrane (for example, Matrigel, Corning Life Sciences)[87] and synthetic or mixed materials such as PEG[88], alginate[89], HA[90], collagen–agarose[91] and alginate–reconstituted basement membrane to simulate different elastic or viscoelastic features of the tumor ECM[10]. The tunable properties include cell–matrix adhesion, pore size, fibrillar structure, organization and degradability. The elastic modulus of 3D gels is controlled either by (1) adjusting the density of the constituent such as collagen[64,92], which may have unwanted secondary effects such as altering signaling pathways that can be sensitive to collagen I density, tension or alignment[93], or (2) enzymatic and chemical changes implemented by fibril cross-linking[67] and physical approaches such as varying the gelation temperature, pH and ultraviolet light treatment[94]. The approach of inhibiting cross-linkers has also been used in vivo to alter the stiffness properties of neoplastic and pre-neoplastic tissues[67]. Ionic or covalent cross-linking of hydrogels could also be used to alter viscoelasticity and the stress relaxation response of the hydrogel[10]. An 'overlay' culture system, also called the 'on-top assay', has been used to benefit from the advantages of both 2D and 3D culture systems[95]. Due to anabolic and catabolic activities of cancer and stromal cells, the material properties of tumors and their surrounding tissue change over time. To simulate the dynamic material properties, hydrogels based on click chemistry with dynamically tunable properties have been proposed[96].

Matrix architecture and cell geometry

Consequences and importance in cancer

Local tissue architecture plays an important role in cancer progression and treatment response, independent of solid stress, fluid forces and stiffness of the microenvironment. The simplest and one of the earliest ways to demonstrate the role of architecture is by comparing 2D to 3D cell culture: when grown within 3D matrices, normal and cancerous breast epithelial cells exhibit markedly distinct morphologies and proliferation rates. However, these differences become challenging to discern when the cells are cultured on 2D surfaces[87]. This is an example of the dynamic reciprocity between tissue function and neoplastic transformation, which alters tissue architecture: cells create their environment but are also affected by it[97]. Another major phenomenon that demonstrates the reciprocity concept is the cancer cell migration capability as the cells actively remodel and sense their surrounding matrix[98]. Studies of 3D matrix architecture, mainly focused on collagen, show that collagen organization is a prognostic biomarker[99] and that certain architectures facilitate cancer cell migration[100]. Using a 3D model system to recapitulate matrix organization, these investigators demonstrated that Rho-associated protein kinase (ROCK)-mediated matrix alignment is a key step in promoting cancer cell migration in the early stages of invasion[101]. Additionally, collagen alignment modulates matrix metalloproteinase-dependent mechanisms[102] and integrin β_1 expression[103], which affect the ability of cells to migrate.

One of the aspects of biology most influenced by tissue architecture is cell geometry, which can affect cell phenotype independent of tissue stiffness or other environmental cues. One of the earliest works that identified the links between cell geometry and its biological responses was reported in 1978 by Folkman and Moscona[104], showing that a reduction in cell substrate contact area reduces DNA synthesis. In another seminal study, Chen and colleagues demonstrated that growth and viability of cells could be controlled by confining cells to micro-patterned islands[105]. In this work, cell growth and apoptosis were shown to be regulated by cell shape, regardless of substrate matrix type or integrin-mediated adhesion[105]. This model system has later been extended to micropillar and nanopillar substrate systems[106] that decouple cell contact area from substrate stiffness (as shown in Fig. 4c) by varying pillar length, width and spacing.

Cell geometry also alters gene expression through changes in nuclear geometry[107,108]. Cells that are more spread out with large contact areas have a more spread out or flattened nucleus; this change of shape has been tied to perinuclear actin and microtubule networks[109]. By altering the contact geometry via a microcontact printing model system, specific chromosomes were shown to change their 3D orientation and arrangement in the nucleus, resulting in differential gene expression[109]. The geometry of the cell and its nucleus is also altered during cell migration through constriction. Migration of cancer cells[107,110,111], immune cells[111] and primary mesenchymal stem cells[110] through pores, which are sometimes smaller than their nucleus size, results in excessive compression and deformation of the nucleus, which leads to loss of integrity of the nuclear envelope and eventually DNA double-strand breaks[107,110,111] and genomic instabilities[110].

Nuclear transcription factors, such as YAP and TAZ, are key players in the genetic program driven by cell geometry, as their regulation is sensitive to cell shape[112]. When breast cancer cells are allowed to spread on large micro-patterned islands coated with fibronectin, YAP and TAZ localize to the nucleus; when they are confined to smaller micro-patterned areas, YAP and TAZ are exported to the cytoplasm. Similar nuclear localization of YAP–TAZ was observed in cells at the edges of epithelial sheets with high curvature, another geometrical parameter. Actomyosin cytoskeleton and Rho GTPase activity were shown to regulate YAP–TAZ activity in response to cell geometry,

similar to the YAP–TAZ response to mechanical stress and stiffness[112]. A variety of biomaterials including synthetic and natural hydrogels in 2D and 3D have been engineered to control YAP–TAZ dependence, which are reviewed in detail in ref. 113.

The migratory response of cancer cells to substrate topography, termed topotaxis, has been studied by the use of nanofabricated substrates, in which the density of the posts and pillars that define the contact geometry alters spatially. Altered topography via such a system was shown to guide the migration of melanoma cells via phosphoinositide-3-kinase (PI3K) and ROCK signaling[114]. The anisotropy of the cell substrate, designed to simulate collagen anisotropy, has also been shown to reduce proliferation of breast epithelial cells (MCF-10A) and induce a temporary dormancy via activation of actomyosin contractility, while having a minimal effect on the proliferation of breast cancer cells as MCF7 and MDA-MB-231 cells[115].

Finally, the links between architecture and function of the tissue surrounding the tumors and how different tumor growth patterns differentially affect this link have been reported recently[41]. Using crystal ribcage, the matrix architecture was imaged in functioning alveoli inside, around and far from metastatic tumors. It was shown that collagen structure is substantially changed from wavy to stretched in a breast cancer lung metastasis with a nodular growth pattern. The tensile stresses that resulted in stretched collagen also altered alveolar and capillary functions in the peritumoral region up to a couple of alveoli into the normal-looking tissue. By contrast, a size-matched breast cancer lung metastasis, formed from another cell line that exhibits an infiltrative growth pattern, did not alter the matrix architecture. The collagen fibers maintained their wavy structure, and alveoli within and surrounding the tumor maintained their functionality. This contrasting effect of nodular versus infiltrative growth on the structure–function of the surrounding alveoli[41], similarly reported in the context of brain tumors[6], demonstrates the importance of growth patterns as a determinant of key physical hallmarks of cancer such as architecture and solid stresses.

Methods of measurement

Histological analysis and second-harmonic generation (SHG) microscopy are the main methods available to characterize cellular geometry and ECM architecture (Fig. 4a)[4,101,116]. SHG imaging is a powerful method that can image collagen I networks in live tissue[41,100,116,117]. As a label-free method, SHG is a powerful tool for longitudinal characterization of tissue architecture at high resolution without the need for fixation and subsequent sectioning. Major matrix components such as collagen I can also be analyzed through immunohistochemistry in paraffin-embedded or frozen samples, and the former is the preferred method as it better preserves tissue architecture. More recently, 3D reconstruction of large tissues up to 3.5 cm^3 from serial histological sections has been reported, and 3D images of normal, precancerous and cancerous human pancreata have been reconstructed at subcellular resolution (Fig. 4b)[118].

Experimental model systems

One of the most used model systems for controlling cell geometry is microcontact printing[105], which restricts cell spreading by patterning the ECM component of interest onto a 2D substrate (Fig. 4c). The shape of the microcontact area can be arbitrarily specified; for example, circular, rectangular or stretched patterns have been used to study cell spreading and cytoskeletal organization, while micro-patterned lines allow studies of one-dimensional migration[119]. Microcontact printing can also be performed on the top of micropillars to study the effects of cell geometry and substrate stiffness simultaneously[120]. Other studies have used grooved substrates to simulate spacing between aligned fibers in tissues[121]. Groove depth and spacing can be tuned from nanometers to micrometers to determine the effects of aspect ratio[122] as well as width and density on cell migration[114] (Fig. 4d). Microfabricated posts with varied spacing[107] and microchannels with widths smaller than a cell nucleus[111] have been used to study nucleus mechanics in cells migrating through constrictions (Fig. 4e–g). Transwell filters with pore sizes smaller than cell nuclei have been used to study cell migration through constrictions and are more practical for analyzing larger numbers of cells[110](Fig. 4h).

In experimental systems, it is possible to control the architecture of the collagen network by adjusting collagen density, gelation temperature and pH[123]. While these models allow researchers to control matrix architecture and have been used to probe the effect of collagen orientation on cellular response, they have some limitations. For example, changing tension or alignment likely also affects stiffness and porosity of the matrix, which may affect cell biology directly or indirectly through altered hydraulic permeability or focal contact dynamics. Macromolecular crowding has been proposed as an improved method for tuning the matrix architecture independent of stiffness and porosity of the matrix[124]. Using PEG as the molecular crowding agent in a collagen gel, it was shown that the resulting matrix has tighter fibrillar networks, and the cells exhibit a less contractile and spreading phenotype[124]. In addition to 3D collagen matrices, the geometry surrounding the cells can be modeled in 3D by the use of microchannels made in polydimethylsiloxane (PDMS)[125]. Other 3D models for simulating the 3D topography and geometrical features of the tumor microenvironment include photopatterned gels[96] and micromolding, which independently tunes matrix stiffness and geometry in 3D[68].

As mentioned in Consequences and importance in cancer, cellular geometry and consequently biological responses change dramatically when cells are cultured in 2D versus 3D. Ex vivo or organoid tumor models are a recent development for studying tumor biology in 3D in which architecture and cellular geometry resemble the tumor more closely than in 2D model systems. These models generally involve one or more cell types cultured in 3D and have been developed for many cancer types including colon, esophagus, pancreas, stomach, liver, endometrium and breast[126]. Organoids are developed by culturing the isolated tumor cells in 3D basement membrane extract and selecting cancer cells with specific inhibitors. The resulting cultures resemble the tumor epithelium both genetically and phenotypically and can be cryopreserved and genetically modified. Despite these advantages, organoid models are very far from in vivo tissues including neoplastic tissues, and the findings would require in vivo validations. Characterization of other physical hallmarks in organoids such as stiffness and solid stress and tuning them in association with pathophysiological values in tumors will benefit the effort in using organoid model systems in cancer research.

Perspective

The tumor microenvironment is distinctively abnormal in both its biological and physical aspects. The growing recognition of the physical microenvironment's importance in cancer research has led to key insights regarding the origins and impacts of its physical characteristics, yielding novel therapeutic targets and strategies for patient treatment. The field of physical sciences in cancer, inherently interdisciplinary, necessitates active collaboration among cancer biologists, clinicians, physical scientists, engineers and data scientists. Understanding the often non-intuitive concepts involved demands a thorough grasp of both physical and biological facets of tumors.

The expansion of physical oncology as a field faces several challenges. Given that these proposed physical hallmarks have been less explored than their biological counterparts, the in vivo and in vitro methods for studying them are currently limited. Therefore, there is a need for more advanced and representative in vivo and in vitro model systems to simulate the prolonged stress exposure experienced by cells. Improved models will help uncover pathways responsive to solid stress and differentiate the biological effects of solid stress from those of other factors, such as increased stiffness. Moreover, there is a need

for enhanced measurement tools to differentiate the various causes and effects of solid stress. Identifying the roles of different factors contributing to solid stress accumulation, like cell–cell and cell–matrix interactions, remains a crucial, unaddressed need that could lead to new therapeutic targets to reduce solid stress in tumors and normalize their physical microenvironment.

We will also need better strategies for reducing solid stress or tissue stiffness in the clinic. Despite being the most extensively studied physical hallmark of tumors, there is a lack of pharmacologic interventions to target stiffness selectively and specifically. Approaches to target the ECM to reduce solid stresses, for example, angiotensin receptor blockers and enzymatic targeting of HA as discussed above, potentially reduce stiffness as well. Open questions include how these strategies affect stiffness in tumors and the pathways associated with it. Dissecting the physical mechanisms (for example, solid stress versus stiffness versus IFP) underlying the outcome of these drugs will inform the development of novel therapeutic strategies.

Similarly, cell micro-architecture is one of the most extensively studied physical hallmarks of cancer, and it has been associated with many cellular responses including proliferation, apoptosis, migration and metabolism, not only in cancer cells but also in stromal cells including endothelial cells, fibroblasts and normal epithelial cells. Despite the immense progress in our basic understanding of the importance of cell geometry, opportunities for translating these concepts into clinical practice have not been identified. One reason for this lack of translation in clinical practice is that currently there are no techniques to accomplish this in vivo or in situ in patients.

Emerging technologies can be used to better understand the causes and the consequences of physical hallmarks of cancer. Such technologies include digital and 3D pathologies, such as CODA[118], with which the hidden third dimension of tumor architecture is now readily available and can be used in archived and fresh clinical and preclinical samples. Another key technology is single-cell omics, which is gradually being used in the context of physical hallmarks of cancer. This technology will have the potential to reveal the highly heterogeneous origins of physical hallmarks of cancer and to delineate the differential effect of each hallmark on the highly diverse cellular constituents of the tumor[127]. Finally, novel model systems, such as whole-organ ex vivo maintenance[41], which combines the controllability of in vitro systems and the complexity of in vivo systems, have the potential to advance our understanding of the physical hallmarks of cancer. These models can modulate and monitor the physics and immunity of tumor cells while preserving whole-organ function, as demonstrated in the context of lung tumors via crystal ribcage[41].

References

1. Nia, H. T., Munn, L. L. & Jain, R. K. Physical traits of cancer. *Science* **370**, eaaz0868 (2020).
   This paper provided a conceptual framework to study the tumor microenvironment by identifying four physical hallmarks of cancer.
2. Linke, J., Munn, L. L. & Jain, R. Compressive stresses in cancer: characterization and implications for tumor progression and treatment. *Nat. Rev. Cancer* **24**, 768–791 (2024).
3. Nia, H. T. et al. Solid stress and elastic energy as measures of tumour mechanopathology. *Nat. Biomed. Eng.* **1**, 0004 (2017).
   This paper provided multiple quantitative methods to measure solid stresses in tumors both ex vivo and in situ.
4. Chauhan, V. P. et al. Angiotensin inhibition enhances drug delivery and potentiates chemotherapy by decompressing tumour blood vessels. *Nat. Commun.* **4**, 2516 (2013).
   This paper demonstrated that a blood pressure-lowering drug that targets angiotensin receptor could lower the solid stress in a solid tumor and improve the outcome of anti-cancer therapy in preclinical models of breast and pancreatic cancer.
5. Stylianopoulos, T. et al. Causes, consequences, and remedies for growth-induced solid stress in murine and human tumors. *Proc. Natl Acad. Sci. USA* **109**, 15101–15108 (2012).
   This paper provided the first experimental evidence of the existence of solid stress in mouse and human tumors.
6. Seano, G. et al. Solid stress in brain tumours causes neuronal loss and neurological dysfunction and can be reversed by lithium. *Nat. Biomed. Eng.* **3**, 230–245 (2019).
   This paper demonstrated that brain tumors with nodular versus infiltrative growth patterns exert different levels of solid stress on the surrounding host tissue and that the high solid stress can kill peritumor neurons.
7. Zhang, S. et al. Intravital measurements of solid stresses in tumours reveal length-scale and microenvironmentally dependent force transmission. *Nat. Biomed. Eng.* **7**, 1473–1492 (2023).
   This paper provided the first in vivo measurement of solid stress in mice and showed that solid stress transmission is scale dependent.
8. Follain, G. et al. Fluids and their mechanics in tumour transit: shaping metastasis. *Nat. Rev. Cancer* **20**, 107–124 (2020).
9. Wirtz, D., Konstantopoulos, K. & Searson, P. C. The physics of cancer: the role of physical interactions and mechanical forces in metastasis. *Nat. Rev. Cancer* **11**, 512–522 (2011).
10. Chaudhuri, O., Cooper-White, J., Janmey, P. A., Mooney, D. J. & Shenoy, V. B. Effects of extracellular matrix viscoelasticity on cellular behaviour. *Nature* **584**, 535–546 (2020).
11. Helmlinger, G., Netti, P. A., Lichtenbeld, H. C., Melder, R. J. & Jain, R. K. Solid stress inhibits the growth of multicellular tumor spheroids. *Nat. Biotechnol.* **15**, 778–783 (1997).
    This paper showed for the first time how compressive solid stresses are linked to cancer cell proliferation, resulting in coining the term 'solid stress' to distinguish mechanical stresses generated by solid constituents of the tumor from the pressure from fluid in a tumor.
12. Padera, T. P. et al. Pathology: cancer cells compress intratumour vessels. *Nature* **427**, 695 (2004).
13. Munn, L. L. & Jain, R. K. Vascular regulation of antitumor immunity. *Science* **365**, 544–545 (2019).
14. Tse, J. M. et al. Mechanical compression drives cancer cells toward invasive phenotype. *Proc. Natl Acad. Sci. USA* **109**, 911–916 (2012).
15. Jones, D. et al. Solid stress impairs lymphocyte infiltration into lymph-node metastases. *Nat. Biomed. Eng.* **5**, 1426–1436 (2021).
16. Fernández-Sánchez, M. E. et al. Mechanical induction of the tumorigenic β-catenin pathway by tumour growth pressure. *Nature* **523**, 92–95 (2015).
17. Murphy, J. E. et al. Total neoadjuvant therapy with FOLFIRINOX in combination with losartan followed by chemoradiotherapy for locally advanced pancreatic cancer: a phase 2 clinical trial. *JAMA Oncol.* **5**, 1020–1027 (2019).
18. Datta, M. et al. Losartan controls immune checkpoint blocker-induced edema and improves survival in glioblastoma mouse models. *Proc. Natl Acad. Sci. USA* **120**, e2219199120 (2023).
19. Zhao, Y. et al. Losartan treatment enhances chemotherapy efficacy and reduces ascites in ovarian cancer models by normalizing the tumor stroma. *Proc. Natl Acad. Sci. USA* **116**, 2210–2219 (2019).
20. Wu, L. et al. Losartan prevents tumor-induced hearing loss and augments radiation efficacy in NF2 schwannoma rodent models. *Sci. Transl. Med.* **13**, eabd4816 (2021).
21. Sherman, M. H. et al. Vitamin D receptor-mediated stromal reprogramming suppresses pancreatitis and enhances pancreatic cancer therapy. *Cell* **159**, 80–93 (2014).

22. Provenzano, P. P. et al. Enzymatic targeting of the stroma ablates physical barriers to treatment of pancreatic ductal adenocarcinoma. *Cancer Cell* **21**, 418–429 (2012).
23. Rahbari, N. N. et al. Anti-VEGF therapy induces ECM remodeling and mechanical barriers to therapy in colorectal cancer liver metastases. *Sci. Transl. Med.* **8**, 360ra135 (2016).
24. Ramanathan, R. K. et al. Phase IB/II randomized study of FOLFIRINOX plus pegylated recombinant human hyaluronidase versus FOLFIRINOX alone in patients with metastatic pancreatic adenocarcinoma: SWOG S1313. *J. Clin. Oncol.* **37**, 1062–1069 (2019).
25. Olive, K. P. et al. Inhibition of Hedgehog signaling enhances delivery of chemotherapy in a mouse model of pancreatic cancer. *Science* **324**, 1457–1461 (2009).
26. Aykut, B. et al. Targeting Piezo1 unleashes innate immunity against cancer and infectious disease. *Sci. Immunol.* **5**, eabb5168 (2020).
27. Jairaman, A. et al. Piezo1 channels restrain regulatory T cells but are dispensable for effector $CD4^+$ T cell responses. *Sci. Adv.* **7**, eabg5859 (2021).
28. Du, H. et al. Tuning immunity through tissue mechanotransduction. *Nat. Rev. Immunol.* **23**, 174–188 (2023).
29. Zhang, S. et al. The peritumor microenvironment: physics and immunity. *Trends Cancer* **9**, 609–623 (2023).
30. Mittelheisser, V. et al. Evidence and therapeutic implications of biomechanically regulated immunosurveillance in cancer and other diseases. *Nat. Nanotechnol.* **19**, 281–297 (2024).
31. Chuong, C.-J. & Fung, Y.-C. In *Frontiers in Biomechanics* 117–129 (Springer, 1986).
32. Nia, H. T. et al. Quantifying solid stress and elastic energy from excised or in situ tumors. *Nat. Protoc.* **13**, 1091–1105 (2018).
33. Dolega, M. E. et al. Cell-like pressure sensors reveal increase of mechanical stress towards the core of multicellular spheroids under compression. *Nat. Commun.* **8**, 14056 (2017).
34. Lee, W. et al. Dispersible hydrogel force sensors reveal patterns of solid mechanical stress in multicellular spheroid cultures. *Nat. Commun.* **10**, 144 (2019).
35. Mohagheghian, E. et al. Quantifying compressive forces between living cell layers and within tissues using elastic round microgels. *Nat. Commun.* **9**, 1878 (2018).
36. Cheng, G., Tse, J., Jain, R. K. & Munn, L. L. Micro-environmental mechanical stress controls tumor spheroid size and morphology by suppressing proliferation and inducing apoptosis in cancer cells. *PLoS ONE* **4**, e4632 (2009).
37. Nam, S. & Chaudhuri, O. Mitotic cells generate protrusive extracellular forces to divide in three-dimensional microenvironments. *Nat. Phys.* **14**, 621–628 (2018).
38. Polacheck, W. J. & Chen, C. S. Measuring cell-generated forces: a guide to the available tools. *Nat. Methods* **13**, 415–423 (2016).
39. Delarue, M. et al. Compressive stress inhibits proliferation in tumor spheroids through a volume limitation. *Biophys. J.* **107**, 1821–1828 (2014).
40. Wagstaff, L. et al. Mechanical cell competition kills cells via induction of lethal p53 levels. *Nat. Commun.* **7**, 11373 (2016).
41. Banerji, R. et al. Crystal ribcage: a platform for probing real-time lung function at cellular resolution in health and disease. *Nat. Methods* **20**, 1790–1801 (2023).
42. Jain, R. K. & Baxter, L. T. Mechanisms of heterogeneous distribution of monoclonal antibodies and other macromolecules in tumors: significance of elevated interstitial pressure. *Cancer Res.* **48**, 7022–7032 (1988).
43. Boucher, Y., Baxter, L. T. & Jain, R. K. Interstitial pressure gradients in tissue-isolated and subcutaneous tumors: implications for therapy. *Cancer Res.* **50**, 4478–4484 (1990).
The first experimental evidence that IFP is uniformly elevated throughout a tumor and drops precipitously in the margin with adjacent normal tissue.
44. Fyles, A. et al. Long-term performance of interstial fluid pressure and hypoxia as prognostic factors in cervix cancer. *Radiother. Oncol.* **80**, 132–137 (2006).
45. Willett, C. G. et al. Direct evidence that the VEGF-specific antibody bevacizumab has antivascular effects in human rectal cancer. *Nat. Med.* **10**, 145–147 (2004).
This paper provided direct evidence that an anti-VEGF antibody can reduce IFP and vascular leakiness in human tumors.
46. Tolaney, S. M. et al. Role of vascular density and normalization in response to neoadjuvant bevacizumab and chemotherapy in breast cancer patients. *Proc. Natl Acad. Sci. USA* **112**, 14325–14330 (2015).
47. Swartz, M. A. & Fleury, M. E. Interstitial flow and its effects in soft tissues. *Annu. Rev. Biomed. Eng.* **9**, 229–256 (2007).
48. Ng, C. P., Hinz, B. & Swartz, M. A. Interstitial fluid flow induces myofibroblast differentiation and collagen alignment in vitro. *J. Cell Sci.* **118**, 4731–4739 (2005).
49. Song, J. W. & Munn, L. L. Fluid forces control endothelial sprouting. *Proc. Natl Acad. Sci. USA* **108**, 15342–15347 (2011).
This paper provides the mechanism underlying angiogenesis controlled by fluid flow shear stresses.
50. Munson, J. M., Bellamkonda, R. V. & Swartz, M. A. Interstitial flow in a 3D microenvironment increases glioma invasion by a CXCR4-dependent mechanism. *Cancer Res.* **73**, 1536–1546 (2013).
51. Polacheck, W. J., Charest, J. L. & Kamm, R. D. Interstitial flow influences direction of tumor cell migration through competing mechanisms. *Proc. Natl Acad. Sci. USA* **108**, 11115–11120 (2011).
52. Swartz, M. A. & Lund, A. W. Lymphatic and interstitial flow in the tumour microenvironment: linking mechanobiology with immunity. *Nat. Rev. Cancer* **12**, 210–219 (2012).
53. Avvisato, C. L. et al. Mechanical force modulates global gene expression and β-catenin signaling in colon cancer cells. *J. Cell Sci.* **120**, 2672–2682 (2007).
54. Jain, R. K. Normalizing tumor microenvironment to treat cancer: bench to bedside to biomarkers. *J. Clin. Oncol.* **31**, 2205–2218 (2013).
55. Boucher, Y., Leunig, M. & Jain, R. K. Tumor angiogenesis and interstitial hypertension. *Cancer Res.* **56**, 4264–4266 (1996).
56. Bera, K. et al. Extracellular fluid viscosity enhances cell migration and cancer dissemination. *Nature* **611**, 365–373 (2022).
57. Netti, P. A., Berk, D. A., Swartz, M. A., Grodzinsky, A. J. & Jain, R. K. Role of extracellular matrix assembly in interstitial transport in solid tumors. *Cancer Res.* **60**, 2497–2503 (2000).
58. Gullino, P. M. The internal milieu of tumors. *Prog. Exp. Tumor Res.* **8**, 1–25 (1966).
59. Chary, S. R. & Jain, R. K. Direct measurement of interstitial convection and diffusion of albumin in normal and neoplastic tissues by fluorescence photobleaching. *Proc. Natl Acad. Sci. USA* **86**, 5385–5389 (1989).
60. Hassid, Y., Furman-Haran, E., Margalit, R., Eilam, R. & Degani, H. Noninvasive magnetic resonance imaging of transport and interstitial fluid pressure in ectopic human lung tumors. *Cancer Res.* **66**, 4159–4166 (2006).
61. Bruns, O. T. et al. Next-generation in vivo optical imaging with short-wave infrared quantum dots. *Nat. Biomed. Eng.* **1**, 0056 (2017).
62. Hadzipasic, M. et al. Emergence of nanoscale viscoelasticity from single cancer cells to established tumors. *Biomaterials* **305**, 122431 (2024).
63. Engler, A. J., Sen, S., Sweeney, H. L. & Discher, D. E. Matrix elasticity directs stem cell lineage specification. *Cell* **126**, 677–689 (2006).
This paper provided the first evidence on how substrate stiffness directs the lineage of stem cells.

64. Paszek, M. J. et al. Tensional homeostasis and the malignant phenotype. *Cancer Cell* **8**, 241–254 (2005).
This paper linked matrix stiffness to cytoskeletal tension through integrins and demonstrated how it regulates the malignant phenotype.
65. Tung, J. C. et al. Tumor mechanics and metabolic dysfunction. *Free Radic. Biol. Med.* **79**, 269–280 (2015).
66. Bordeleau, F. et al. Matrix stiffening promotes a tumor vasculature phenotype. *Proc. Natl Acad. Sci. USA* **114**, 492–497 (2017).
67. Levental, K. R. et al. Matrix crosslinking forces tumor progression by enhancing integrin signaling. *Cell* **139**, 891–906 (2009).
68. Pathak, A. & Kumar, S. Independent regulation of tumor cell migration by matrix stiffness and confinement. *Proc. Natl Acad. Sci. USA* **109**, 10334–10339 (2012).
69. Alvarez, R. et al. Stromal disrupting effects of nab-paclitaxel in pancreatic cancer. *Br. J. Cancer* **109**, 926–933 (2013).
70. Miroshnikova, Y. A. et al. Tissue mechanics promote IDH1-dependent HIF1α–tenascin C feedback to regulate glioblastoma aggression. *Nat. Cell Biol.* **18**, 1336–1345 (2016).
71. Acerbi, I. et al. Human breast cancer invasion and aggression correlates with ECM stiffening and immune cell infiltration. *Integr. Biol.* **7**, 1120–1134 (2015).
72. Leight, J. L., Wozniak, M. A., Chen, S., Lynch, M. L. & Chen, C. S. Matrix rigidity regulates a switch between TGF-β1-induced apoptosis and epithelial–mesenchymal transition. *Mol. Biol. Cell* **23**, 781–791 (2012).
73. Wang, W. et al. Diabetic hyperglycemia promotes primary tumor progression through glycation-induced tumor extracellular matrix stiffening. *Sci. Adv.* **8**, eabo1673 (2022).
74. Boyd, N. F. et al. Evidence that breast tissue stiffness is associated with risk of breast cancer. *PLoS ONE* **9**, e100937 (2014).
75. Maskarinec, G. et al. Mammographic density as a predictor of breast cancer survival: the multiethnic cohort. *Breast Cancer Res.* **15**, R7 (2013).
76. Choi, S. et al. Bone-matrix mineralization dampens integrin-mediated mechanosignalling and metastatic progression in breast cancer. *Nat. Biomed. Eng.* **7**, 1455–1472 (2023).
77. Chaudhuri, O. et al. Hydrogels with tunable stress relaxation regulate stem cell fate and activity. *Nat. Mater.* **15**, 326–334 (2016).
78. Han, Y. L. et al. Cell contraction induces long-ranged stress stiffening in the extracellular matrix. *Proc. Natl Acad. Sci. USA* **115**, 4075–4080 (2018).
79. LeBourdais, R. et al. Mapping the strain-stiffening behavior of the lung and lung cancer at microscale resolution using the crystal ribcage. *Front. Netw. Physiol.* **4**, 1396593 (2024).
80. Shao, X. et al. MatrisomeDB 2.0: 2023 updates to the ECM–protein knowledge database. *Nucleic Acids Res.* **51**, D1519–D1530 (2023).
81. Hajjarian, Z. et al. Laser speckle rheology for evaluating the viscoelastic properties of hydrogel scaffolds. *Sci. Rep.* **6**, 37949 (2016).
82. Scarcelli, G. et al. Noncontact three-dimensional mapping of intracellular hydromechanical properties by Brillouin microscopy. *Nat. Methods* **12**, 1132–1134 (2015).
83. Regan, K. et al. Multiscale elasticity mapping of biological samples in 3D at optical resolution. *Acta Biomater.* **176**, 250–266 (2023).
84. Masuzaki, R. et al. Assessing liver tumor stiffness by transient elastography. *Hepatol. Int.* **1**, 394–397 (2007).
85. Venkatesh, S. K. et al. MR elastography of liver tumors: preliminary results. *AJR Am. J. Roentgenol.* **190**, 1534–1540 (2008).
86. Weigelt, B., Ghajar, C. M. & Bissell, M. J. The need for complex 3D culture models to unravel novel pathways and identify accurate biomarkers in breast cancer. *Adv. Drug Deliv. Rev.* **69–70**, 42–51 (2014).
87. Petersen, O. W., Ronnov-Jessen, L., Howlett, A. R. & Bissell, M. J. Interaction with basement membrane serves to rapidly distinguish growth and differentiation pattern of normal and malignant human breast epithelial cells. *Proc. Natl Acad. Sci. USA* **89**, 9064–9068 (1992).
88. Peyton, S. R., Raub, C. B., Keschrumrus, V. P. & Putnam, A. J. The use of poly(ethylene glycol) hydrogels to investigate the impact of ECM chemistry and mechanics on smooth muscle cells. *Biomaterials* **27**, 4881–4893 (2006).
89. Huebsch, N. et al. Harnessing traction-mediated manipulation of the cell/matrix interface to control stem-cell fate. *Nat. Mater.* **9**, 518–526 (2010).
90. Khetan, S. et al. Degradation-mediated cellular traction directs stem cell fate in covalently crosslinked three-dimensional hydrogels. *Nat. Mater.* **12**, 458–465 (2013).
91. Ulrich, T. A., Jain, A., Tanner, K., MacKay, J. L. & Kumar, S. Probing cellular mechanobiology in three-dimensional culture with collagen–agarose matrices. *Biomaterials* **31**, 1875–1884 (2010).
92. Provenzano, P. P., Inman, D. R., Eliceiri, K. W. & Keely, P. J. Matrix density-induced mechanoregulation of breast cell phenotype, signaling and gene expression through a FAK–ERK linkage. *Oncogene* **28**, 4326–4343 (2009).
93. Engler, A. et al. Substrate compliance versus ligand density in cell on gel responses. *Biophys. J.* **86**, 617–628 (2004).
94. Tibbitt, M. W. & Anseth, K. S. Hydrogels as extracellular matrix mimics for 3D cell culture. *Biotechnol. Bioeng.* **103**, 655–663 (2009).
95. Lee, G. Y., Kenny, P. A., Lee, E. H. & Bissell, M. J. Three-dimensional culture models of normal and malignant breast epithelial cells. *Nat. Methods* **4**, 359–365 (2007).
96. DeForest, C. A. & Anseth, K. S. Cytocompatible click-based hydrogels with dynamically tunable properties through orthogonal photoconjugation and photocleavage reactions. *Nat. Chem.* **3**, 925–931 (2011).
97. Nelson, C. M. & Bissell, M. J. Modeling dynamic reciprocity: engineering three-dimensional culture models of breast architecture, function, and neoplastic transformation. *Semin. Cancer Biol.* **15**, 342–352 (2005).
98. Sahai, E. & Marshall, C. J. Differing modes of tumour cell invasion have distinct requirements for Rho/ROCK signalling and extracellular proteolysis. *Nat. Cell Biol.* **5**, 711–719 (2003).
99. Conklin, M. W. et al. Aligned collagen is a prognostic signature for survival in human breast carcinoma. *Am. J. Pathol.* **178**, 1221–1232 (2011).
100. Provenzano, P. P. et al. Collagen reorganization at the tumor–stromal interface facilitates local invasion. *BMC Med.* **4**, 38 (2006).
101. Provenzano, P. P., Inman, D. R., Eliceiri, K. W., Trier, S. M. & Keely, P. J. Contact guidance mediated three-dimensional cell migration is regulated by Rho/ROCK-dependent matrix reorganization. *Biophys. J.* **95**, 5374–5384 (2008).
102. Fraley, S. I. et al. Three-dimensional matrix fiber alignment modulates cell migration and MT1-MMP utility by spatially and temporally directing protrusions. *Sci. Rep.* **5**, 14580 (2015).
103. Velez, D. O. et al. 3D collagen architecture induces a conserved migratory and transcriptional response linked to vasculogenic mimicry. *Nat. Commun.* **8**, 1651 (2017).
104. Folkman, J. & Moscona, A. Role of cell shape in growth control. *Nature* **273**, 345–349 (1978).
105. Chen, C. S., Mrksich, M., Huang, S., Whitesides, G. M. & Ingber, D. E. Geometric control of cell life and death. *Science* **276**, 1425–1428 (1997).
This paper provided the first evidence of how geometry, distinct from stiffness, can regulate cell life and death.

106. Tan, J. L. et al. Cells lying on a bed of microneedles: an approach to isolate mechanical force. *Proc. Natl Acad. Sci. USA* **100**, 1484–1489 (2003).
107. Denais, C. M. et al. Nuclear envelope rupture and repair during cancer cell migration. *Science* **352**, 353–358 (2016).
This paper was among the first to show how passage of cells through constricted geometries can cause nucleus deformation and DNA damage.
108. Cho, S., Irianto, J. & Discher, D. E. Mechanosensing by the nucleus: from pathways to scaling relationships. *J. Cell Biol.* **216**, 305–315 (2017).
109. Ramdas, N. M. & Shivashankar, G. V. Cytoskeletal control of nuclear morphology and chromatin organization. *J. Mol. Biol.* **427**, 695–706 (2015).
110. Irianto, J. et al. DNA damage follows repair factor depletion and portends genome variation in cancer cells after pore migration. *Curr. Biol.* **27**, 210–223 (2017).
111. Raab, M. et al. ESCRT III repairs nuclear envelope ruptures during cell migration to limit DNA damage and cell death. *Science* **352**, 359–362 (2016).
112. Dupont, S. et al. Role of YAP/TAZ in mechanotransduction. *Nature* **474**, 179–183 (2011).
113. Brusatin, G., Panciera, T., Gandin, A., Citron, A. & Piccolo, S. Biomaterials and engineered microenvironments to control YAP/TAZ-dependent cell behaviour. *Nat. Mater.* **17**, 1063–1075 (2018).
114. Park, J. et al. Directed migration of cancer cells guided by the graded texture of the underlying matrix. *Nat. Mater.* **15**, 792–801 (2016).
115. Chaudhuri, P. K., Pan, C. Q., Low, B. C. & Lim, C. T. Topography induces differential sensitivity on cancer cell proliferation via Rho–ROCK–myosin contractility. *Sci. Rep.* **6**, 19672 (2016).
116. Brown, E. et al. Dynamic imaging of collagen and its modulation in tumors in vivo using second-harmonic generation. *Nat. Med.* **9**, 796–800 (2003).
117. Perentes, J. Y. et al. In vivo imaging of extracellular matrix remodeling by tumor-associated fibroblasts. *Nat. Methods* **6**, 143–145 (2009).
118. Kiemen, A. L. et al. CODA: quantitative 3D reconstruction of large tissues at cellular resolution. *Nat. Methods* **19**, 1490–1499 (2022).
119. Maiuri, P. et al. Actin flows mediate a universal coupling between cell speed and cell persistence. *Cell* **161**, 374–386 (2015).
120. Wong, S., Guo, W. H. & Wang, Y. L. Fibroblasts probe substrate rigidity with filopodia extensions before occupying an area. *Proc. Natl Acad. Sci. USA* **111**, 17176–17181 (2014).
121. Kim, D.-H., Provenzano, P. P., Smith, C. L. & Levchenko, A. Matrix nanotopography as a regulator of cell function. *J. Cell Biol.* **197**, 351–360 (2012).
122. Wisniewski, E. O. et al. Dorsoventral polarity directs cell responses to migration track geometries. *Sci. Adv.* **6**, eaba6505 (2020).
123. Wolf, K. et al. Physical limits of cell migration: control by ECM space and nuclear deformation and tuning by proteolysis and traction force. *J. Cell Biol.* **201**, 1069–1084 (2013).
124. Ranamukhaarachchi, S. K. et al. Macromolecular crowding tunes 3D collagen architecture and cell morphogenesis. *Biomater. Sci.* **7**, 618–633 (2019).
125. Stroka, K. M. et al. Water permeation drives tumor cell migration in confined microenvironments. *Cell* **157**, 611–623 (2014).
126. Drost, J. & Clevers, H. Organoids in cancer research. *Nat. Rev. Cancer* **18**, 407–418 (2018).
127. Baysoy, A., Bai, Z., Satija, R. & Fan, R. The technological landscape and applications of single-cell multi-omics. *Nat. Rev. Mol. Cell Biol.* **24**, 695–713 (2023).
128. Campas, O. et al. Quantifying cell-generated mechanical forces within living embryonic tissues. *Nat. Methods* **11**, 183–189 (2014).
129. Zheng, S. et al. Alteration of mechanical stresses in the murine brain by age and hemorrhagic stroke. *PNAS Nexus* **3**, 141 (2024).
130. Benham-Pyle, B. W., Pruitt, B. L. & Nelson, W. J. Mechanical strain induces E-cadherin-dependent Yap1 and β-catenin activation to drive cell cycle entry. *Science* **348**, 1024–1027 (2015).
131. Serwane, F. et al. In vivo quantification of spatially varying mechanical properties in developing tissues. *Nat. Methods* **14**, 181–186 (2017).
132. Ricca, B. L. et al. Transient external force induces phenotypic reversion of malignant epithelial structures via nitric oxide signaling. *eLife* **7**, e26161 (2018).
133. Barr, R. G., Memo, R. & Schaub, C. R. Shear wave ultrasound elastography of the prostate: initial results. *Ultrasound Q.* **28**, 13–20 (2012).
134. Xu, L. et al. Magnetic resonance elastography of brain tumors: preliminary results. *Acta Radiol.* **48**, 327–330 (2007).
135. Chauvet, D. et al. In vivo measurement of brain tumor elasticity using intraoperative shear wave elastography. *Ultraschall Med.* **37**, 584–590 (2016).
136. Streitberger, K. J. et al. High-resolution mechanical imaging of glioblastoma by multifrequency magnetic resonance elastography. *PLoS ONE* **9**, e110588 (2014).
137. Plodinec, M. et al. The nanomechanical signature of breast cancer. *Nat. Nanotechnol.* **7**, 757–765 (2012).
138. Théry, M. et al. The extracellular matrix guides the orientation of the cell division axis. *Nat. Cell Biol.* **7**, 947–953 (2005).

Acknowledgements

This work was supported in part by the National Cancer Institute (R01-CA259253, R01-CA208205, R01-NS118929, U01-CA261842, U01-CA 224348), an Outstanding Investigator Award (R35-CA197743 to R.K.J.), R01-CA204949 and R01-HL128168 to L.L.M. and R21EB031332, DP2HL168562, a Beckman Young Investigator Award, an NSF CAREER Award, a Kilachand Fund Award, a Sloan Research Fellowship and DoD HT9425241053 to H.T.N. R.K.J.'s research is also supported by grants from the National Foundation for Cancer Research, the Nile Albright Research Foundation, the Harvard Ludwig Center, Jane's Trust Foundation and the Bill and Melinda Gates Foundation and Boehringer Ingelheim and Sanofi.

Author contributions

H.T.N., L.L.M. and R.K.J. conceived and jointly wrote the Review.

Competing interests

R.K.J. received consultant and/or SAB fees from Cur, DynamiCure, Elpis, Merck and SynDevRx; owns equity in Accurius, Enlight and SynDevRx; and served on the boards of trustees of Tekla Healthcare Investors, Tekla Life Sciences Investors, Tekla Healthcare Opportunities Fund and Tekla World Healthcare Fund. The Massachusetts General Hospital has applied for patents related to concepts discussed in this Review. L.L.M. receives equity from Bayer and is a consultant for SimBioSys. The remaining author declares no competing interests.

Additional information

Correspondence and requests for materials should be addressed to Hadi T. Nia, Lance L. Munn or Rakesh K. Jain.

Peer review information *Nature Methods* thanks Konstantinos Konstantopoulos and the other, anonymous, reviewer(s) for their contribution to the peer review of this work. Primary Handling Editor: Madhura Mukhopadhyay, in collaboration with the *Nature Methods* team.